

# Development of a Robotic Rat Hindlimb Model

Evan Aronhalt<sup>1(⊠)</sup>, Eabha Abramson<sup>1</sup>, Clarus Goldsmith<sup>2</sup>, Emanuel Andrada<sup>3</sup>, William Nourse<sup>4</sup>, Gregory Sutton<sup>5</sup>, Nicholas Szczecinski<sup>2</sup>, and Roger Quinn<sup>1</sup>

- Department of Mechanical and Aerospace Engineering, Case Western Reserve University, Cleveland, OH 44106, USA era32@case.edu
- $^2\,$  Department of Mechanical and Aerospace Engineering, West Virginia University, Morgantown, WV 26505, USA
- <sup>3</sup> Institute of Zoology and Evolutionary Research, Friedrich-Schiller University, Jena, Germany
  - Department of Electrical, Computer, and Systems Engineering, Case Western Reserve University, Cleveland, OH 44106, USA
    - School of Life Sciences, University of Lincoln (UK), Brayford Pool, Lincoln LN6 7TS, UK

Abstract. This paper discusses the design decisions, process, and results for a set of robotic rat hindlimbs scaled up to 2.5 times the size of the rat. The design is inspired by a previous model from within our lab, but includes a variety of improvements to further the utility and biological accuracy of the model. The robot is comprised of two legs with four motors each to actuate sagittal rotations of the hip, knee, and ankle joints as well as an internal hip rotation. The motor's torque, inertial, viscous, and stiffness properties are characterized for dynamic scaling to be properly implemented in the future control scheme. With direct position commands, the robot's joint movements are able to reflect those of the rat, proving its validity as a test bed for the implementation of future neural control schemes.

**Keywords:** Rat hindlimb · Robot · Dynamic scaling

### 1 Introduction

Robot locomotion capabilities are continuously advancing. Robots today are better able to traverse complex environments through advanced mechanical design

This work was supported by NSF RI 1704436 and also DFG FI 410/16-1 and NSF DBI 2015317 as part of the NSF/CIHR/DFG/FRQ/UKRI-MRC Next Generation Networks for Neuroscience Program.

<sup>©</sup> The Author(s), under exclusive license to Springer Nature Switzerland AG 2023 F. Meder et al. (Eds.): Living Machines 2023, LNAI 14158, pp. 115–130, 2023. https://doi.org/10.1007/978-3-031-39504-8\_8

and control schemes. One source of inspiration for robot design is the animal kingdom. Animals have evolved over many years to navigate through a variety of environments with relative ease, a capability that is still being developed and perfected in robots. Several robots that have taken inspiration from biology are Drosophibot, Puppy, and MIT Cheetah 3, based on the fruit fly, whippet, and cheetah, respectively [2,8,10].

Outside of the lab's previous hindlimb model and a model produced by Shi et al. [7,15], rat robots have yet to be explored in great depth. A rat is a prime candidate for a biologically inspired robot for a variety of reasons. A robot with the locomotion ability of a rat could have many practical uses. Furthermore, rat data is both readily available and easily acquired if needed due to the commonality of testing on rats. In addition, there are few legged robots with a similar dynamic scale to rats, which makes it interesting from a scientific perspective. This paper discusses the design decisions for and philosophies behind the design of a set of robotic rat hindlimbs.

# 2 Design

#### 2.1 Previous Iteration

A previous robotic rat hindlimb model was developed by Emmett Donnelley-Power, from which inspiration was taken and a variety of design decisions were kept, shown in Fig. 1 [7].

This robot has two legs each with three degrees of freedom consisting of sagittal plane rotation at the hip, knee, and ankle. The limbs are approximated by rods, and they are actuated by Dynamixel MX-64 and AX-12A servo motors (Robotis, Seoul, South Korea). The two legs are connected by a connector piece located where the pelvis would exist. This connector piece is then free to translate vertically but not horizontally or rotationally through the rod in the center of the assembly and the two drawer slides in the back. The mount allows for self-supported walking movements without the system actually moving forward, removing the need for a treadmill or wheels. The basic principles of this robot, i.e. using motors to control each joint, approximate robot size, serial control, and general mount design, were carried over to the new design.

## 2.2 Limb and Joint Design

The new robot described in this paper consists of two legs with three limb segments each: the femur, tibia, and foot, a pelvis, and an electronics mount on top. Each leg has 4 degrees of freedom: sagittal rotation at the hip, knee, and ankle, and femoral long axis rotation at the hip. The decision to use these 4 degrees of freedom was informed by experimentally gathered data of joint angles during rat trot as well as data from Dienes et al.'s paper on 3 dimensional rat hindlimb walking analysis [6].

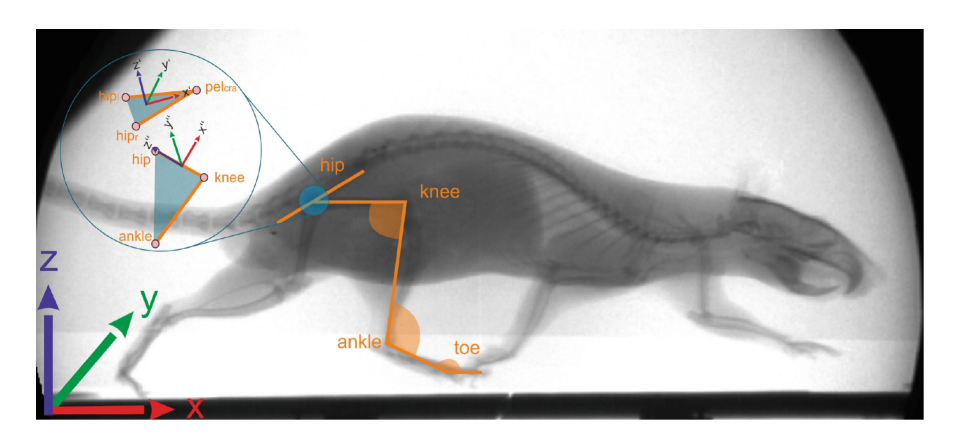
In our experiments, which were approved by the Committee for Animal Research of the State of Thuringia, Germany (registry number: 02-060/16),



Fig. 1. Robot rat hindlimb model created by Emmett Donnelley-Power. One should note the center fixture where the pelvis should be, as this is one of the larger changes in the updated model. The fixture on this model tended to lean backwards, as the slider joints connected to each motor would easily become loose. Also, the fixture was much wider than the pelvis would have been, leading to inaccuracy in the limb placement. In addition, one can see that all of the limb segments are in plane with each other. In the animal, the limb segments share parallel planes, but are slightly out of plane with each other.

rats moved across a 2.3 m walking track, at their preferred speeds. Body and limb kinematics were collected by using a bi-planar high-speed x-ray fluoroscope (Neurostar, Siemens, Erlangen, Germany) and two synchronized standard light high-speed cameras (SpeedCam Visario g2, Weinberger, Erlangen, Germany) at 500 Hz. X-ray raw video data was first undistorted (batchUndistort routine, www.xromm.org). Manual digitization of the landmarks was performed in SimiMotion (SimiMotion Systems, Unterschleißheim, Germany). Knee, ankle and metatarsophalangeal joint angles were computed as three-point angles. To estimate the three-dimensional rotations occurring at the hip, we computed the relative Cardian angles (x-y-z) between the pelvis and a plane formed by the hip joint, the knee joint and the ankle joint (Fig. 2), for further information see [1].

The three sagittal plane rotations were chosen as they all have a range of motion greater than  $60^{\circ}$  (Fig. 3). Thus, they were all deemed essential for three dimensional walking. The hip is the logical next place to add degrees of freedom to allow locomotion out of the sagittal plane. Changes in the hip joint position



**Fig. 2.** X-ray image of a rat during trot. Superimposed are the analyzed body segments and joint angles. Knee, ankle and metatarsophalangeal joint angles were computed as three-point angles. Hip three-dimensional rotations were estimated by computing the Cardian angles between the pelvis (composed by both hip joints and the pelvis cranial marker) and a plane formed by the hip joint, the knee joint, and the ankle joint.

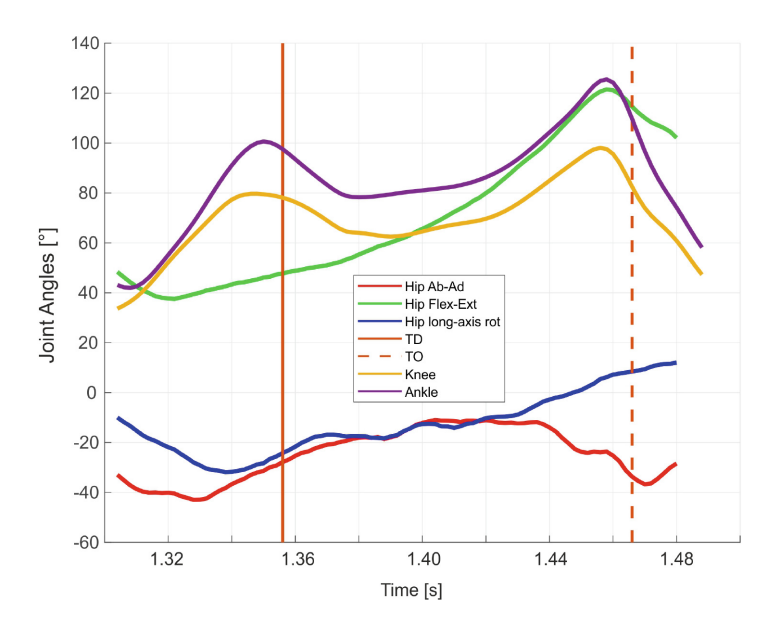


Fig. 3. Joint angle data for the rat hindlimb over one step. Assuming that the knee, and ankle mainly work as revolute joints, the motion of the plane formed by the hip, knee and ankle relative to the pelvis display three-dimensional hip kinematics. Ab-Ad: abduction/adduction. Flex-Ext: flexion/extension. TD: touch-down, TO: toe-off. Positive Hip Flex-Ext values indicate hip extension. Positive values in long axis rotation indicate femoral internal rotation while the foot is moved towards lateral. Positive Ab-Ad values indicate adduction.

have the greatest effect on limb placement during gait due to the joint's placement at the beginning of the leg chain. As such, changes in hip position move the entire leg and can have a great effect on foot movement. In addition, the second degree of freedom found in the knee joint of a rat is barely noticeable, and the other degrees of freedom in the ankle joint are used primarily for foot stability [12].

Only one other joint was included due to space limitations on the robot, increased robot mass, and diminishing returns in accuracy for increased design complexity. The hip internal and external rotation was chosen over hip abduction and adduction due to it having an overall greater range of motion. The data from Dienes et al. shows hip internal rotation having a range of motion of approximately 30° compared to the hip adduction range of motion of 10° [6]. However, abduction/adduction may be important to the hindlimb locomotion, and the effects of these rotations will be explored in future work.

The limbs were created from 3 dimensional models by Hunt et al. [11] and adapted into Solidworks 3D model files (Solidworks Corp., Waltham, MA). The choice to create the limbs in the shape of rat bones instead of an arbitrary shape was guided by several factors. The primary reason was that all attachment points between limb segments could be easily placed where they are found in the animal. In addition, force transfer within the limb segments would be slightly more accurate to the animal since the position of the joints is accurate. This only applies to the joint reaction force, and only partially, as the lack of musculature greatly changes the force distribution of the system.

The foot design had to be changed due to a lack of structural integrity in the bony foot model. The current foot is longer and thicker than an actual rat foot would be, with a slight convex curvature to help with sliding along the ground (Fig. 4). This behavior is normally accounted for by the metatarsophalangeal joints which were omitted from the design for the sake of reducing complexity [18].



Fig. 4. Comparison between new (left) and old (right) foot design.

The robot is 2.5 times larger than a female Sprague-Dawley rat. Limb segment length data were obtained from Johnson et al. [12]. This length scale was chosen for practical purposes. It is easier to work with components at this scale and the high efficiency motor/transmissions were available for this robot size.

For the sagittal plane attachment points, the driving motor is mounted on the proximal limb segment using a circular mounting face. For example, the motor driving the tibia is mounted at the bottom of the femur. The limb segment being driven is attached to the driving motor via the motor's shaft by a hole in the limb segment with a flat to match that of the motor shaft. This connection is then secured by placing a bolt through a hole on the flat of the motor shaft and limb segment hole, minimizing slip between the shaft and limb segment.

The hip internal rotation motors were mounted onto the pelvis. A connector piece and a bracket were then used to mount this motor and the hip sagittal rotation motor. The hip internal rotation motors were raised vertically so that the final position of the hip sagittal rotation axis matched that in the animal. In addition, careful attention was given to making sure the axes of rotation of these two joints intersected to create a partial ball-and-socket joint instead of two separate rotational joints, meaning that the two rotational axes intersected throughout the entire gait cycle. Finally, the ball of the femur and the socket of the hip were used to position the limb at the correct location. Both attachments are shown in Fig. 5.

All structural components were printed using the Markforged Mark Two 3D printer (Markforged, Watertown, MA). They were primarily made with the

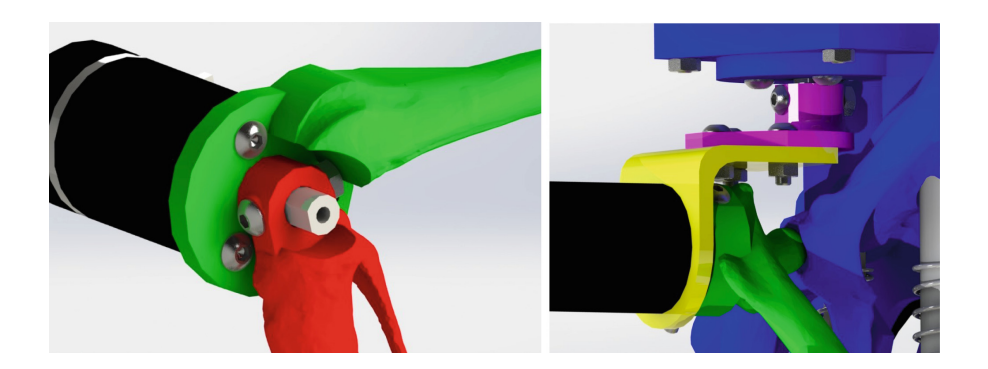


Fig. 5. Left: Attachment between the femur (green) and tibia (red) at the knee joint. The motor driving the tibia is attached to the previous limb segment (the femur) securely by the circular pattern of three screws shown in the picture. The motor shaft is secured to the tibia both by the flat seen on the shaft and the hole as well as the screw and nut seen travelling through the tibia and motor shaft; utilizing both of these methods minimizes slippage of the shaft when driving the tibia. Right: Hip assembly for the left leg. The sagittal hip rotation motor, driving the femur (green), is attached to the L bracket (yellow), which is then attached to the connector piece (pink) that is driven by the motor responsible for the internal and external rotation of the hip. That motor is attached to the pelvis (blue). (Color figure online)

company's proprietary filament, Onyx, with the addition of varying amounts of carbon fiber supports. All limb segments were carbon fiber reinforced since they will be transferring the forces of walking. The bracket, connector piece, and bottom of the pelvis were also fully reinforced to hold the weight of an entire leg assembly. Carbon fiber was omitted from the top of the pelvis and in the electronics mount, since these areas will be lightly loaded.

The electronics mount is attached to the top of the pelvis and houses the eight electronic speed controllers used by the motors, the power board, and the Controller Area Network (CAN) board, where all eight motors' CAN cables are connected. CAN will be discussed in the Sect. 2.3. All motors are powered by one off-board 24 V power supply and communicate with an Arduino Teensy 4.0 Microcontroller (PJRC, Sherwood, USA) located slightly off-board the robot.

The mount was designed similarly to the one used in Donnelly-Power's robot; it allows for self-supported walking movements while keeping the robot in place by restraining the pelvis with a rod and spring to provide support and allow vertical motion through clamping the base. However, only one rod was used instead of a rod with drawer rails to reduce friction. In addition, a bearing was put inside of the pelvis during printing to further reduce friction during walking. The full Solidworks assembly is shown in Fig. 6.

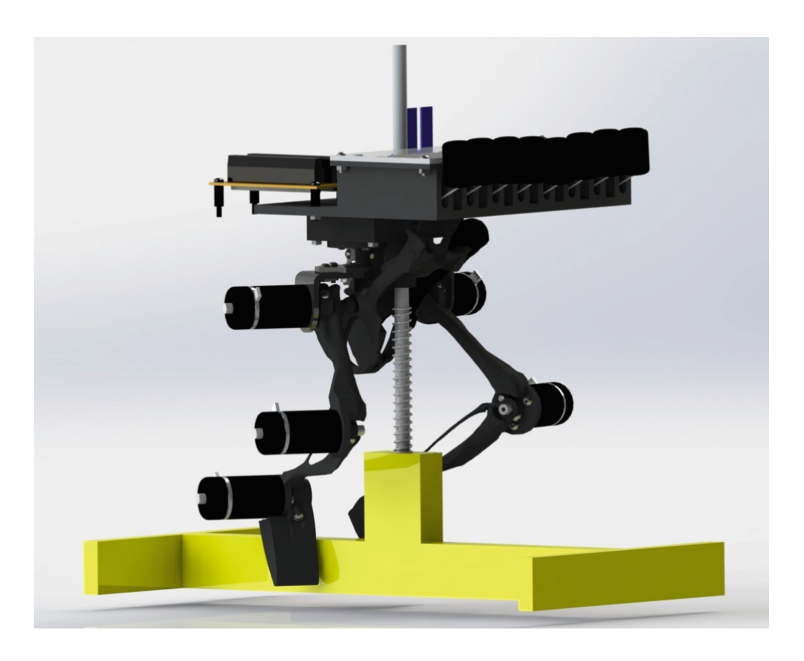


Fig. 6. Full rat hindlimbs and pelvis model in Solidworks with electronics. The bars on the mount are for the stability of the robot, particularly during the limb pushing against the ground. The electronics at the top include the CAN and power boards near the back of the robot and the eight speed controllers housed near the front.

#### 2.3 Motor Testing and Characterization

Despite rats using 38 muscles in their hind legs [19], electric motors were chosen as the actuators for the robot for practical purposes. Artificial muscles such as McKibbens have many advantages in terms of more closely modeling the animal [10]. However, they also have many disadvantages, such as requiring an air compressor and valves. Thus, it is easier to develop an autonomous robot to run outside of the lab using motors, which is the end goal of this project.

The previous model also uses motors, but instead uses Dynamixel MX-64 and AX-12A motors (Robotis, Seoul, South Korea). We decided against using Dynamixels for this project because we desired greater torque, greater backdrivability and better feedback.

We chose Robomaster M2006 (DJI, Shenzhen, China) motors with C610 speed controllers for all joints in the robot. These motors use the Controller Area Network (CAN) bus protocol to communicate with each other and the Teensy microcontroller (PJRC, Sherwood, USA). CAN bus is a form of serial communication where the motors are connected to each other instead of needing to all be individually connected to the microcontroller [3].

The main low level control software, written in C++, runs on the microcontroller and continually sends commands to the motors over the CAN bus. While connected to a serial interface, the microcontroller can accept current commands for the motors and transmit them over the CAN bus, or it can accept position commands and hold the motors in place using a PID control loop. The header files that allow communication with the motors over the CAN bus were developed by the Stanford Robotics Club [13]. The control gains for the microcontroller's onboard PID control loop are P = 100,000, I = 5,000, and D = 10,000. These values were hand-tuned to minimize rise time and overshoot while maintaining good position-holding capabilities.

The Robomaster motors have several desirable qualities that led to them being chosen over other options. Backdrivability was an important factor, as the limbs and thus the motors will constantly be changing direction during gait. Form factor also influenced the decision to use the Robomaster motors. The M2006's have a small diameter front face compared to other "pancake-shaped" motors. This smaller face size allows for easier integration of the motors into the robot.

Current control was the primary reason for using the Robomaster motors, due to torque control being important in locomotion. While the Robomaster motors do not possess the capability of direct torque control, it can be approximated by using current control and establishing a current-to-torque relationship. The manufacturer specifications claim that the motor has a torque constant of approximately 0.2 Nm/A (DJI, Shenzhen, China). To confirm this, a testing procedure was developed to measure the torque the motor produces when commanded a specific current value. A rod was attached to the motor output shaft about its end. Then, a current command was sent so that the motor would begin to rotate. The rod would then collide with a scale, from which the scale reading would be converted to a force, and then that force converted to a torque based

on the rod length. This process was repeated for different currents, starting at  $0\,\mathrm{A}$  and increasing by  $0.1\,\mathrm{A}$  until reaching  $3.5\,\mathrm{A}$ . The motor's rated maximum continuous current is  $3\,\mathrm{A}$ . The final torque constant obtained through experimentation was  $0.2657\,\mathrm{Nm/A}$ , with Fig. 7 showing all of the tests. This is a 32.85% increase from the manufacturer specified torque constant.

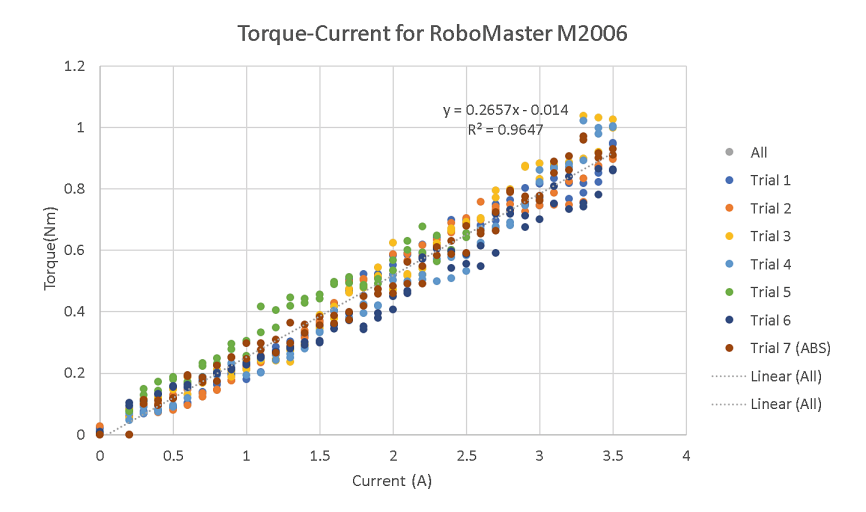


Fig. 7. Experimental torque vs. current relationship for the RoboMaster M2006 motor.

In this paper, the robot is controlled by animal joint angles being given as position commands to the motors. This is done to test the design and strength of the robot.

The manufacturer specifications of the motor claim the motors can produce 1 Nm of maximum continuous torque. We discovered that the maximum torque the motor could produce was just over 1 Nm at stall. If the limb is fully extended, the gravitational torque on the hip sagittal motor will be 0.58 Nm, which is slightly greater than half of the stall torque. This extreme scenario would not occur during normal walking; the gravitational torque seen would be less, thus we believe the motors will have sufficient torque.

In addition to the current-to-torque relationship, other quantities need to be measured to facilitate correct dynamic scaling: the motor's internal moment of inertia from the rotor  $(J_{motor})$ , damping coefficient from electromagnetic field effects in the coils  $(c_{motor})$ , and stiffness from the proportional gain of the PID loop  $(k_{motor})$ . The testing procedure utilized for this characterization is similar to that used for Drosophibot [8]. For  $J_{motor}$  and  $c_{motor}$ , this process involves attaching a weighted pendulum to the motor and recording the motor's position during freely rotating pendulum oscillations. These oscillation tests were conducted both while the motor was non-powered and while the motor was powered with no commanded position set. Both the damping and stiffness require power to the motor to be present, so removing power isolates the effects of  $J_{motor}$  in the

setup. Powering the motor without a commanded position then adds damping into the system without adding stiffness, as the PID loop is not utilized. The exact mass placed at the end of the pendulum varied depending on the test conducted. For inertia testing, a mass of  $500\,\mathrm{g}$  was used to minimize inertia of the pendulum and make the motor's inertia easier to measure. For damping tests, a mass of  $1000\,\mathrm{g}$  was used to increase the number of oscillations so that  $c_{motor}$  could be more easily measured.

Using the angle vs. time data from the pendulum trials, the experimentally observable properties of the oscillations were leveraged to derive  $J_{motor}$  and  $c_{motor}$ . Namely, the damped natural frequency  $(\omega_d)$  and the logarithmic decrement  $(\delta)$  were utilized:

$$\omega_d = \omega_n \sqrt{1 - \zeta^2} \tag{1}$$

$$\delta = ln \frac{\theta_1}{\theta_2} = \frac{2\pi \cdot c_{motor}}{\omega_d \cdot 2m} \tag{2}$$

where  $\omega_n$  is the natural frequency,  $\zeta$  is the damping ratio,  $\theta_1$  and  $\theta_2$  are the heights of the two adjacent oscillation peaks, and m is the total mass of the pendulum setup.  $\omega_n$  and  $\zeta$  can be calculated as:

$$\omega_n = \sqrt{\frac{k_{system}}{J_{system}}} = \sqrt{\frac{k_{pend}}{J_{motor} + J_{pend}}}$$
 (3)

$$\zeta = \frac{\delta}{(2\pi)^2 + \delta^2} \tag{4}$$

where  $k_{pend}$  is the stiffness of the pendulum due to gravity:

$$k_{pend} = g \cdot m \cdot L_{pend} \tag{5}$$

And  $J_{pend}$  is the pendulum's moment of inertia:

$$J_{pend} = m \cdot L_{pend}^2 \tag{6}$$

 $L_{pend}$  is the length of the pendulum. Equations 3–6 can be substituted into Eqs. 1 and 2, and the equations reordered to produce equations to solve for  $J_{motor}$  and  $c_{motor}$  from easily calculated or observed quantities:

$$J_{motor} = \frac{k_{pend}}{\omega_d^2} \left(1 - \frac{\delta}{\sqrt{(2\pi)^2 + \delta^2}}\right) - J_{pend} \tag{7}$$

50 inertia trials and 50 damping trials were recorded, then MATLAB (The MathWorks, Natick, Massachusetts) scripts were used to compile and evaluate the data. A moment of inertia of  $J_{motor} = 0.00392 \pm 0.00188 \, \mathrm{kgm^2}$  (47.9% error), a damping ratio of  $\zeta = 0.119 \pm 0.0109$  (9.20% error), and a damping coefficient of  $1.617 \pm 0.146 \, \mathrm{Ns/m}$  (9.03% error) were calculated.

This testing procedure was developed for Dynamixel servos, which can monitor their sensory components without powering the motor. Robomaster M2006 motors do not have a manner with which to do this while the motor is powered

off, resulting in damping being present during the inertia tests. This issue contributes to the error in the calculated inertia, and will be addressed in future tests by using point tracking in video recordings instead of relying on the motor's sensory components.

Stiffness testing is based on the angular application of Hooke's law to the pendulum:

$$\tau = k_{motor} \Delta \theta \tag{8}$$

where  $\Delta\theta$  is the difference between the commanded angle of the motor  $(\theta_{com})$  and actual angle  $(\theta_{act})$ , and  $\tau$  is the torque produced by the motor. The pendulum was positioned to press down on a scale such that a  $\Delta\theta$  was produced. The scale reading was then converted to a torque value based on the pendulum length. This process was repeated for several commanded positions (and thus different  $\Delta\theta$  values) to create a  $\tau$  vs  $\Delta\theta$  curve.  $k_{motor}$  was then calculated as the linear slope of this curve. After 5 trials, the stiffness of the motor under the present PID controller was found to be 8.40 Nm/rad.

#### 2.4 Dynamic Scaling

The goal is for the robot to move dynamically similar to the rat. Animals of different length and dynamics require different forces to drive their locomotion. For example, insect locomotion is dominated by viscous moments during the swing phase of the limb and elastic forces to hold the limb in place during stance phase, similar to how a spring behaves [9]. Large mammal locomotion is dominated by the inertial forces of the limb following the muscle activation at the start of swing phase.

To be scaled accurately, first the forces active during rat swing phase and stance phase must be characterized; the same distribution of torques must then be present in the robotic model. Young et al. discusses the distribution of rat hindlimb torques at the hip joint below, at, and above rat scale [20]. At rat scale, the ground reaction force, or load, is dominating the muscle torque response. At horse scale, inertia is dominating the muscle torque. In their work, Young et al. use the correlation coefficient to determine the relative contribution of forces to the hip joint torques. Gravitational forces play slightly more of a role in smaller scale animals than larger animals, but are mostly overpowered by other forces at both scales. As such, the correlation coefficient may overstate the importance of gravitational forces, but remains a valuable resource to convey the impact of scale on torque contributions from viscoelastic vs. inertial forces.

At the rat scale, inertial forces have a relative contribution of 0.7 to the hip joint torques, whereas the viscoelastic forces have a relative torque contribution of -0.6, where a correlation of positive 1 means it completely dominates the motion, and a correlation of negative 1 means it does not affect the motion at all. Looking at the robot scale of 2.5 times the size of the rat, the linear correlation coefficient for inertial forces increases to 0.9, and the viscoelastic and gravitational forces decrease to about -0.8. As the size of the rat increases, the system becomes more inertially dominated. However, the desired locomotion

behavior of the robot is that of a rat at true scale, not at 2.5 times scale, meaning the inertial forces of the robot model must be decreased to more accurately reflect the original size rat.

Presently, the motor's motion is stiffness dominated, as the motor's stiffness greatly outweighs its damping and inertia. This is not accurate to the rat's load dominated movement, but can be altered by changing parameters in the PID controller. The PID controller gains are currently set high to achieve a quick response, which means the motor stiffness is similarly high. The motor stiffness was further tested, this time decreasing the P gain from 100,000 to 50,000, which in turn resulted in a stiffness of 5.40 N/m compared to the previous 8.40 N/m. Further testing is required to obtain a stiffness value low enough that will result in locomotion that is more accurate to that of the rat and to see how low the stiffness can be without affecting robot performance. If a low enough stiffness is not practical, increasing the walking speed will shift the system towards being more inertially dominated [9]. Matching these dynamic properties will lead to the correct driving forces of locomotion, and subsequently the correct overall kinematics.

## 3 Results

Using position feedback, the commanded and actual positions were compared in the left leg, shown in Fig. 8. At this scale, there is no perceptible deviation from the commanded positions, which are the rat locomotion data on a 2.5 times time scale. This is to be expected, as these positions are being directly commanded

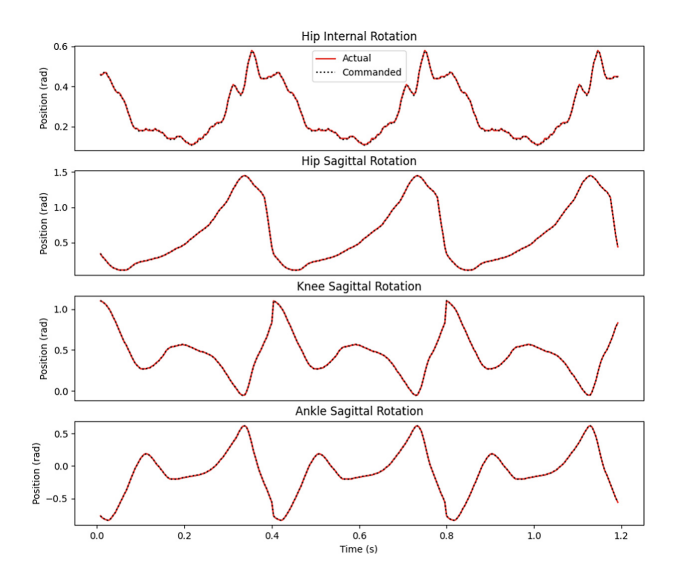


Fig. 8. Commanded and actual joint angles. Commanded joint angles are the animal joint angles at a 2.5 times time scale.

to the motor with high gains in a PID controller. This helps validate the model as being structurally sound and ready to use with future controllers by showing it is capable of reaching the rat hindlimb's range of motion. Further testing is required to ensure that the robot joint angles match those of the animal defined in the coordinate system in Fig. 3.

A video of the robot walking with commanded joint angles can be seen here: https://youtube.com/shorts/l7PZNlQlln8?feature=share, with a picture of the robot in Fig. 9.

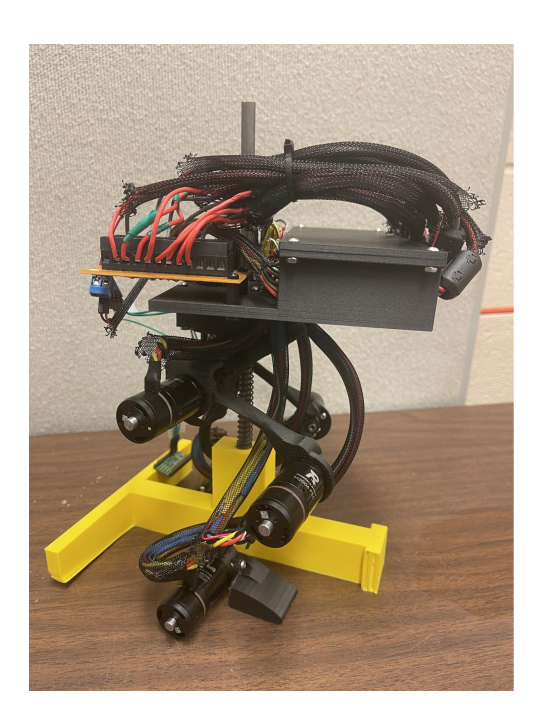


Fig. 9. Present model of the robotic rat hindlimbs.

#### 4 Discussion and Conclusions

In this work, a robot model of rat hindlimbs was created. The model was designed based on animal data scaled up in length by a factor of 2.5. The leg segments were 3D printed using continuous strands of carbon fiber for strength. They are models of the rat bones. The robot limb segment connections are designed to provide direct transmission of the motor output and maintain structural integrity. The hindlimbs are capable of the rat's range of motion during normal walking, with sagittal plane rotations at the hip, knee, and ankle, and a hip internal rotation, for a total of four joints in each leg. Robomaster M2006 motor's are used to

actuate all of the joints. The motor's internal moment of inertia, damping, and stiffness were experimentally characterized under the present control scheme to provide data that will be used for future dynamic scaling. Using a PID controller, the leg joints can move as commanded.

Despite the simplifications of reducing the overall degrees of freedom in the hip, ankle, and metatarsophalangeal joints, the robot was able to produce a gait that matched the joint angles of the animal. This proves the robot to be a sufficient testbed for future control schemes.

There are several other improvements and iterations to be made to the model in the future. The first and most important addition will be the implementation of a synthetic nervous system (SNS) to control the hindlimbs. SNS apply models of animal nervous systems to robotic control [17].

An SNS will be used for the robotic rat hind legs that is based on the twolayer central pattern generator (CPG) model proposed by Rybak et al. and further tested and developed by Deng et al. [4,5,14]. The two layer model allows for independent control of the CPG's oscillation frequency and the motorneuron patterning. The Deng et al. SNS will be tested on this robot. A model proposed by Song et al. which uses groups of slow, intermediate, and fast V2a interneurons to change the speed of locomotion and may be more accurate to vertebrate spinal control will be explored in future work [16].

While achieving SNS control for the robot is the next primary goal, there are other small improvements that could be made to improve the model. A compliant foot could help offset the errors in toe position that arise from treating the foot as a completely rigid body and removing the metatarsophalangeal joints. A possible design inspiration could come from Drosophibot, which uses a rigid tendon moving through the foot segments connected to a spring to create a compliant foot mechanism [8]. This design mimics the feet seen in insects and not mammals, but basic principles could still be adapted to a different design for a rat. The test stand is sufficient to test early stages of the hindlimb walking, but more in depth testing will require the robot to actually use its walking to provide forward locomotion. This will require a tether to above a treadmill.

**Acknowledgements.** We would like to thank Emmett Donnelly-Power for his help in understanding the design philosophy behind his previous rat hindlimb robot. We would also like to thank Fletcher Young for providing data used for the scaling analysis.

# References

- Andrada, E., et al.: Limb, joint and pelvic kinematic control in the quail coping with steps upwards and downwards. Sci. Rep. 12(1), 15901 (2022). https://doi. org/10.1038/s41598-022-20247-y
- Bledt, G., Powell, M.J., Katz, B., Di Carlo, J., Wensing, P.M., Kim, S.: MIT cheetah 3: design and control of a robust, dynamic quadruped robot. Other repository, January 2019. Accessed 17 Aug 2020. ISBN: 9781538680940. Publisher: Institute of Electrical and Electronics Engineers (IEEE)
- 3. Corrigan, S.: Introduction to the Controller Area Network (CAN), May 2016. https://www.ti.com/lit/pdf/sloa101

- Deng, K., et al.: Biomechanical and sensory feedback regularize the behavior of different locomotor central pattern generators. Biomimetics 7(4), 226 (2022). https:// doi.org/10.3390/biomimetics7040226
- Deng, K., et al.: Neuromechanical model of rat hindlimb walking with two-layer CPGs. Biomimetics 4(1), 21 (2019). https://doi.org/10.3390/biomimetics4010021
- Dienes, J., Hicks, B., Slater, C., Janson, K.D., Christ, G.J., Russell, S.D.: Comprehensive dynamic and kinematic analysis of the rodent hindlimb during over ground walking. Sci. Rep. 12(1), 19725 (2022). https://doi.org/10.1038/s41598-022-20288-3
- Donnelley-Power, E.: Design of a rat hindlimb robot and neuromechanical controller. Master's thesis, Case Western Reserve University, Cleveland, Ohio, January 2022
- Goldsmith, C., Szczecinski, N., Quinn, R.: Drosophibot: a fruit fly inspired biorobot. In: Martinez-Hernandez, U., et al. (eds.) Living Machines 2019. LNCS (LNAI), vol. 11556, pp. 146–157. Springer, Cham (2019). https://doi.org/10.1007/978-3-030-24741-6\_13
- Hooper, S.L., et al.: Neural control of unloaded leg posture and of leg swing in stick insect, cockroach, and mouse differs from that in larger animals. J. Neurosci. 29(13), 4109–4119 (2009). https://doi.org/10.1523/JNEUROSCI.5510-08.2009
- Hunt, A., Szczecinski, N., Quinn, R.: Development and training of a neural controller for hind leg walking in a dog robot. Front. Neurorobot. 11, 18 (2017). https://doi.org/10.3389/fnbot.2017.00018
- Hunt, A.J., Szczecinski, N.S., Andrada, E., Fischer, M., Quinn, R.D.: Using animal data and neural dynamics to reverse engineer a neuromechanical rat model. In: Wilson, S.P., Verschure, P.F.M.J., Mura, A., Prescott, T.J. (eds.) LIVING-MACHINES 2015. LNCS (LNAI), vol. 9222, pp. 211–222. Springer, Cham (2015). https://doi.org/10.1007/978-3-319-22979-9-21
- Johnson, W.L., Jindrich, D.L., Roy, R.R., Reggie Edgerton, V.: A three-dimensional model of the rat hindlimb: musculoskeletal geometry and muscle moment arms. J. Biomech. 41(3), 610–619 (2008). https://doi.org/10.1016/j.jbiomech.2007.10.004
- 13. Kau, N.: DJI C610 + M2006 interface library, November 2022. Original-date: 20 September 2020
- Rybak, I.A., Shevtsova, N.A., Lafreniere-Roula, M., McCrea, D.A.: Modelling spinal circuitry involved in locomotor pattern generation: insights from deletions during fictive locomotion: modelling spinal circuitry involved in locomotor pattern generation. J. Physiol. 577(2), 617–639 (2006). https://doi.org/10.1113/jphysiol. 2006.118703
- 15. Shi, Q., et al.: Development of a small-sized quadruped robotic rat capable of multimodal motions. IEEE Trans. Robot. **38**(5), 3027–3043 (2022). https://doi. org/10.1109/TRO.2022.3159188. conference Name: IEEE Transactions on Robotics
- Song, J., et al.: Multiple rhythm-generating circuits act in tandem with pacemaker properties to control the start and speed of locomotion. Neuron 105(6), 1048–1061 (2020). https://doi.org/10.1016/j.neuron.2019.12.030
- Szczecinski, N.S., Hunt, A.J., Quinn, R.D.: A functional subnetwork approach to designing synthetic nervous systems that control legged robot locomotion. Front. Neurorobot. 11, 37 (2017). https://doi.org/10.3389/fnbot.2017.00037
- 18. Varejão, A.S.P., et al.: Motion of the foot and ankle during the stance phase in rats: rat ankle angle during stance. Muscle Nerve **26**(5), 630–635 (2002). https://doi.org/10.1002/mus.10242

- 19. Young, F., Rode, C., Hunt, A., Quinn, R.: Analyzing moment arm profiles in a full-muscle rat hindlimb model. Biomimetics 4(1), 10 (2019). https://doi.org/10. 3390/biomimetics4010010
- 20. Young, F.R., Chiel, H.J., Tresch, M.C., Heckman, C.J., Hunt, A.J., Quinn, R.D.: Analyzing modeled torque profiles to understand scale-dependent active muscle responses in the hip joint. Biomimetics **7**(1), 17 (2022). https://doi.org/10.3390/biomimetics7010017